Case Studies in Thermal Engineering 85 (2026) 108381

Contents lists available at ScienceDirect

Case Studies in Thermal Engineering

journal homepage: www.elsevier.com/locate/csite

Experimental analysis of thermal energy storage using phase change material for photovoltaic and thermal systems

Ye-Bin Shin [a,b], Deuk-Won Kim [a], Wangje Lee [a], Jae-Weon Jeong [b], Min-Hwi Kim [a,*]

[a] Renewable Energy System Laboratory, Korea Institute of Energy Research, 152 Gajeong-ro, Yuseong-gu, Daejeon, 34129, Republic of Korea
[b] Department of Architectural Engineering, College of Engineering, Hanyang University, 222, Wangsimni-Ro, Seongdong-Gu, Seoul, 04763, Republic of Korea

GRAPHICAL ABSTRACT

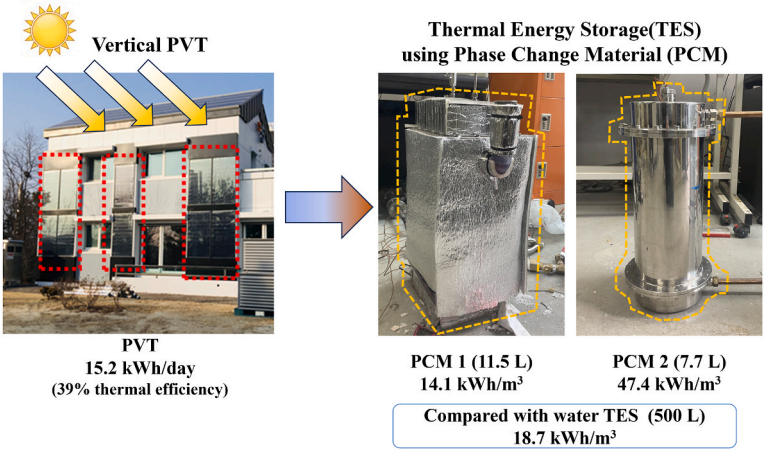

ARTICLE INFO

Keywords:
Phase change materials
Thermal energy storage
Photovoltaic and thermal system

ABSTRACT

This study conducted an experimental case study on the performance of water-based thermal energy storage (WTES) and prototype phase change material (PCM)-based thermal energy storage systems (TES) integrated with a photovoltaic thermal (PVT) system under real operating conditions. Long-term experimental measurements were conducted over two months using a building-

* Corresponding author.
E-mail address: mhkim001@kier.re.kr (M.-H. Kim).

https://doi.org/10.1016/j.csite.2026.108381
Received 22 January 2026; Received in revised form 20 July 2026; Accepted 25 July 2026
Available online 27 July 2026
2214-157X/© 2026 The Authors. Published by Elsevier Ltd. This is an open access article under the CC BY-NC license (http://creativecommons.org/licenses/by-nc/4.0/).

scale PVT system, where thermal input varied dynamically owing to changes in solar irradiance and system operation.

In this study, a conventional WTES connected to an actual PVT system and two prototype PCM-based TESs with different internal piping structures were installed, and the thermal charging and discharging behavior of each storage tank was experimentally analyzed. In addition, the thermal storage amount, storage density, and charging rates were compared based on the inlet and outlet temperatures and flow rates of each system. The average thermal energy collected by the PVT system was 15.2 kWh, of which 9.4 kWh was stored in the WTES, whereas 0.2 kWh and 0.4 kWh were stored in the prototype PCM1-and prototype PCM2-based TES units, respectively. The thermal storage densities were 18.7 kWh/m^3 for the WTES, 14.1 kWh/m^3 for the prototype PCM1-based TES, and 47.4 kWh/m^3 for the prototype PCM2-based TES. In particular, the prototype PCM2-based storage tank with an improved internal piping structure showed higher thermal storage density than PCM1. However, the charging and discharging rates of prototype PCM-based storage tanks were found to be insufficient for real-time thermal buffers under actual PVT operating conditions. The average charging rate of the PCM-based storage tanks was 0.1 kW, compared to 2.6 kW for the WTES. This slow dynamic response constitutes the major limitations of the PCM-based thermal storage concept as tests in this study. This study provided data for the design direction of storage tanks for building applications.

Nomenclature

Symbols	
A	Area, m^2
C_p	Specific heat of fluid, kJ/kg °C
G	Solar irradiance, kW/m^2
I	Solar insolation intensity, W/m^2
m	Mass flow rate, kg/s
Q	Heat gain, kWh
T_{in}	Inlet temperature, °C
T_{out}	Outlet temperature, °C
V	Volume flow rate, m^3/s
Greek symbols	
η_Q	Thermal efficiency
ρ	Density, kg/m^3
δ_{vr}	Type An uncertainty
δ_{ve}	Type B uncertainty
δ_v	Combined uncertainty
σ_Q	Standard deviation
Abbreviations	
GSHP	Ground source heat pump
HEX	Heat exchanger
PVT	Photovoltaic thermal
PCM	Phase change material
TES	Thermal energy storage
WTES	Water-based thermal energy storage

1. Introduction

Owing to recent climate change, restrictions on fossil fuel use and the importance of renewable energy have increased. To reduce the use of fossil fuels and carbon emissions, increasing the share of renewable energy, which serves as an alternative to fossil fuels, has become a global trend [1]. Renewable energy includes solar, hydropower, and geothermal energy. In the building sector, interest has recently increased in photovoltaic thermal (PVT) systems that simultaneously produce electricity and heat from the same area as photovoltaic systems and solar thermal systems installed on building roofs and façades [2]. When PVT systems are applied to buildings, electricity and thermal energy can be produced on-site and self-consumed, thereby increasing self-consumption and reducing dependence on external electricity and thermal energy supplies [3,4]. Therefore, PVT systems play a key role in achieving zero-energy buildings.

When a PVT system is applied to a building, differences may occur between the time of electricity and heat production and the time of energy consumption within the building. Electricity can be exported to the power grid or stored using an energy storage system (ESS). In contrast, thermal energy is typically stored using a thermal storage tank and released during periods of thermal demand [5]. Therefore, thermal energy storage (TES) systems play an essential role in compensating for the irregular energy production of PVT systems [6], [7]. Conventional thermal storage tanks are typically water-based thermal energy storage (WTES). Existing WTES store heat using the sensible heat of water. They are harmless to the human body because they use water, rendering them suitable for large-capacity storage [8], [9].

However, conventional TES, which are suitable for large-capacity storage, are accompanied by a large volume and load owing to the low energy density of sensible heat. This imposes installation constraints when a PVT system is applied to multi-unit residential

environments with limited indoor space. In addition, in residential environments, a mismatch occurs between the periods of PVT heat production and the periods of the occupants' actual heating and hot water demand; therefore, a compact buffer tank that can effectively link the two is essential. Accordingly, a latent heat thermal storage tank utilizing phase change material (PCM), which has a high thermal energy density, is presented as a promising alternative.

Meanwhile, PCMs, which utilize latent heat, have been used in various fields. In the building sector in particular, PCMs are combined with and applied to heat exchangers such as pillow plates to enhance heat-transfer efficiency, and they are integrated as thermal storage solutions into walls, floors, ceilings, and windows to lower indoor peak temperatures and reduce HVAC energy, thereby improving the energy efficiency and sustainability of buildings [10], [11]. Despite such extensive use in the building sector, PCM-based thermal storage tanks still present several challenges that must be overcome. PCMs have a slow heat-transfer capability, which delays the thermal response rate during the charging and discharging processes and prevents an immediate response to real-time thermal loads [12]. For PCM-based thermal storage tanks to perform an effective buffer-tank role under actual operating conditions, design improvements that optimize the internal piping structure or secure a sufficient heat-transfer area are required.

However, most previous studies have focused on performance evaluation of the thermal storage tank rather than on integrating thermal storage tanks with PVT systems.

Studies on PCM-based thermal storage tanks have mainly focused on experimental or simulation environments with constant supply temperatures, and studies on the performance of WTES and PCM-based thermal storage tanks under actual building operation conditions are limited. To evaluate the applicability of PCM-based thermal storage tanks, thermal storage capacity, charging rates, and storage density must be analyzed. Through such analysis, thermal storage tanks with appropriate capacity and performance for PVT systems can be selected. PVT systems do not supply a constant amount of energy during operation but exhibit real-time variations in thermal energy production owing to factors such as solar irradiance, cloud conditions, ambient temperature, and installation angle [13], [14]. Considering these characteristics, analyzing whether appropriate thermal charging and discharging can be achieved in response to real-time variations in collected thermal energy and thermal demand is necessary.

Previous studies have investigated the application of PCM to PVT systems from various perspectives, including PV temperature reduction [15], thermal storage enhancement [16–19], charging and discharging behavior, heat-transfer improvement [20], and the stabilization of thermal energy utilization under intermittent solar conditions [21]. Building on the research gaps identified above [10, 11], this study aims to address the limited investigation of PCM-based thermal storage under realistic PVT operating conditions [22–24] and the lack of comparative analysis of PCM-based thermal storage tanks. Accordingly, to overcome the spatial constraints within multi-unit residential buildings, prototype PCM-based thermal storage tanks were installed in a PVT system, and their real-time thermal behavior was experimentally examined. This study analyzes the thermal behavior of PCM-based thermal storage tanks coupled with a PVT system installed in an actual building under dynamically varying ambient and solar irradiance conditions, in which the collected heat fluctuates in real time. In addition, the charging and discharging performance, where surplus heat collected during the daytime is stored and used to respond to the nighttime thermal load, was experimentally quantified in terms of thermal storage capacity, storage density, and charging time [24–31]. Furthermore, by comparing two storage tanks employing the same PCM material, the influence of internal fin design structures on thermal storage performance [32,33] was experimentally validated, thereby extending the scope of previous research on the thermal network of charging and discharging systems [34–36]. However, this study focuses on identifying the behavior of PCM-based thermal storage tanks under PVT operating conditions and evaluating their charging and discharging performance, rather than improving the material properties of PCM or optimizing storage-tank design [37]. Therefore, material or storage-tank design improvements, such as the application of nanoparticles [38] or the optimization of internal fin structures to enhance the heat-transfer capability of the PCM itself [39], are outside the scope of this study. Furthermore, the evaluation of material-related durability, such as phase-change stability and detailed morphological changes of the PCM associated with repeated charging and discharging cycles, is also excluded from the scope of this study. The prototype PCM-based thermal storage tanks developed in this study were not intended to provide generalized design guidelines for PCM-based thermal storage systems, but rather to serve as a case study investigating the application of PCM to thermal storage tanks under actual PVT operating conditions. In other words, the initial prototype tanks were experimentally examined to evaluate their thermal storage behavior and performance under PVT operating conditions when PCM was applied to the thermal storage system.

2. System description and experimental setup

2.1. Building overview

The experiment was conducted at Energy Plus Solar House (KePSH-2), located within the Korea Institute of Energy Research (KIER) in Daejeon, Republic of Korea [40–42]. This building is one of the facilities of the urban, renewable-energy-based plus energy community within KIER, namely the KIER Plus Energy Community (KPEC).

KePSH-2, used in this study, is a residential building equipped with a PVT system and a ground source heat pump (GSHP). A building-integrated photovoltaic (BIPV) system with a power capacity of 8.3 kWp is installed on the rooftop at a tilt angle of 30°, and vertical PVT modules with a power capacity of 3.3 kWp are installed on the building façade [43]. This study analyzed the performance of PCM-based TES tanks within the energy flow in which thermal energy collected from the vertical PVT system is stored in thermal storage tanks and supplied to the ground heat source. KePSH-2 is a reinforced concrete structure consisting of one basement floor and three above-ground floors, with a building footprint area of 107 m^2 and a total floor area of 266.7 m^2. The installed heat pump has a capacity of 3 RT, with a rated cooling output of 2.3 kW and a heating output of 3.1 kW, and is connected to a 150 m-long ground heat exchanger.

The vertical PVT system of this building is installed on the south-facing exterior wall and comprises crystalline silicon (c-Si) PV cells covered with glass. Each module measures 1040 mm × 2003 mm × 58 mm, with a total installation area of 20 m^2. The module efficiency is 15.9%, with an electrical efficiency of 9.7% and a thermal efficiency of 17.7%. The PVT modules are flat-plate, use a glycol–water mixture as the working fluid, with a mass flow rate of 0.046 kg/s per module.

As shown in Fig. 1, this study utilized the vertical PVT system installed at KePSH-2 for heat source production and the associated buffer TES. The buffer TES employed an existing WTES to enable comparative performance analysis with prototype PCM-based thermal storage tanks. The prototype PCM-based thermal storage tanks were configured in two different types for the experimental investigation.

2.2. Thermal circuit configuration and control logic

Fig. 2 shows the schematic of the thermal circuit used in this study. Thermal energy produced by the vertical PVT system is stored in a WTES and charged into two PCM-based thermal storage tanks. In the prototype PCM-based storage tanks, during charging, water enters through the upper pipe, melts the PCM to store heat, and then exits through the lower pipe. During discharging, the system was designed such that PCM solidifies and releases energy through a bypass pipe branched from the pipes connected to the upper and lower parts of the PCM storage tank. The thermal energy stored in the thermal storage tanks is supplied to the ground heat exchanger through a heat exchanger and heat pump. In other words, the HEX stores the heat produced by the PVT and transfers it to the heat pump and the ground. It was installed such that the water and antifreeze flowing inside the PVT piping did not mix with the refrigerant of the heat pump and only exchanged heat.

In the actual heat flow, the heat discharged from each storage tank is transferred to the ground heat exchanger through the HEX, and finally stored in or released to the ground. The stored heat is discharged again in winter and supplied to the building for heating or hot water through the heat pump, whereas in summer, heat is released to the ground and cooling is performed through the heat pump. During the experimental period from April to June, the heat stored in the storage tanks was transferred to the ground (HEX charging), and the cooled water was returned to the PVT panels.

The calculation equations used in this study are as follows. The thermal energy collected by the PVT system is expressed in Eq. (1), and the inlet temperatures of the WTES and the two prototype PCM-based thermal storage tanks are identical and defined as $T_{PVT\ out}$. The thermal energy produced by the PVT system is denoted as Q_{PVT} with a unit of MJ, and the heat generated when the valve connecting the inlet and outlet is closed was excluded from the calculation. $T_{PVT\ in}$ and $T_{PVT\ out}$ represent the inlet and outlet temperatures, respectively, m_{PVT} is the mass flow rate of the PVT system, and C_P is the specific heat capacity.

$$Q_{PVT} = m_{PVT} \times C_p \times (T_{PVT\ out} - T_{PVT\ in}) \tag{1}$$

The equation used in this study is expressed in Eq. (2). T_{avg} represents the average inlet and outlet temperature of each system.

$$C_p = \frac{-203.606 + 1523.29 \times \left(\frac{T_{avg}+273.15}{1000}\right) - 3196.41\left(\frac{T_{avg}+273.15}{1000}\right)^2 + 2474.455 \times \left(\frac{T_{avg}+273.15}{1000}\right)^3 + \frac{3.855326}{\left(\frac{T_{avg}+273.15}{1000}\right)^2}}{18.0153} \tag{2}$$

The solar irradiance G is calculated using Eq. (3), where I represents the solar irradiance per unit area, and the total area of the PVT system is 20 m^2. The thermal collection efficiency (η_Q) is expressed by Eq. (4).

$$G = \frac{I \times A}{1000} \tag{3}$$



Fig. 1. Overview of test site.

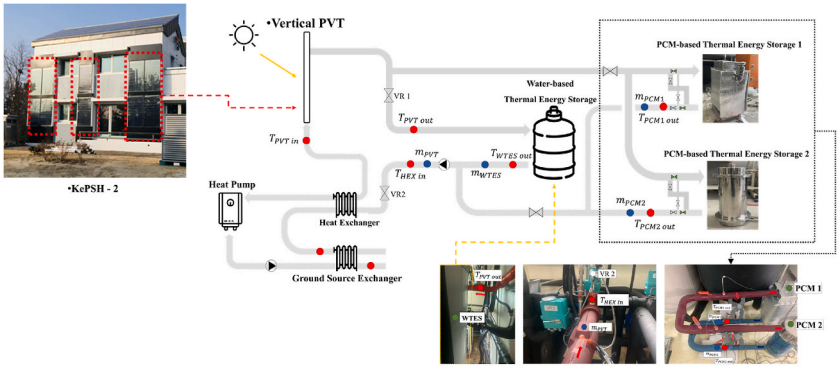

Fig. 2. Components and sensors of test systems.

$$\eta_Q = \frac{Q_{PVT}}{G} \times 100 \tag{4}$$

The thermal charging amount is defined as a positive value, and the thermal discharging amount as a negative value. The thermal charging and discharging amounts of the prototype PCM 1 thermal storage tank and the prototype PCM 2 thermal storage tank are denoted as Q_{PCM1} and Q_{PCM2}, respectively, and are expressed by Eqs. (5) and (6), respectively; the outlet temperatures are $T_{PCM1\ out}$ and $T_{PCM2\ out}$, and the mass flow rates are m_{PCM1} and m_{PCM2}, respectively.

$$Q_{PCM1} = m_{PCM1} \times C_P \times (T_{PCM1\ out} - T_{PVT\ out}) \tag{5}$$

$$Q_{PCM2} = m_{PCM2} \times C_P \times (T_{PCM2\ out} - T_{PVT\ out}) \tag{6}$$

The thermal charging and discharging amount of the WTES is denoted as Q_{WTES}, where the outlet temperature is $T_{WTES\ out}$ out, and the mass flow rate is m_{WTES}. These two data points are virtual sensor values. The m_{PVT} flow rate used to obtain m_{WTES} corresponds to the flow rate at the point where the pipelines distributed to each thermal storage tank merge again. According to the law of energy conservation of the first law of thermodynamics, the flow rate in the entire system, m_{PVT}, and the flow rates branched from m_{PVT} to each storage tank m_{WTES}, m_{PCM1}, and m_{PCM2} were considered.

$$m_{WTES} = m_{PVT} - m_{PCM1} - m_{PCM2} \tag{7}$$

$$T_{HEX\ in} \times m_{PVT} = (T_{PCM\ out} \times m_{PCM1}) + (T_{PCM\ out} \times m_{PCM2}) + (T_{WTES\ out} \times m_{WTES}) \tag{8}$$

$$Q_{WTES} = m_{WTES} \times C_p \times (T_{PVT\ out} - T_{WTES\ out}) \tag{9}$$

Q_{HEX} represents the thermal energy supplied to the ground heat exchanger, and the mass flow rate is m_{PVT}. The inlet and outlet temperatures are $T_{HEX\ in}$ and $T_{HEX\ out}$, respectively.

$$Q_{HEX} = m_{PVT} \times C_P \times (T_{HEX\ out} - T_{HEX\ in}) \tag{10}$$

The capacity of the WTES was 500 L, whereas the capacities of the prototype PCM-based thermal storage tanks were 11.51 L for PCM1 and 7.71 L for PCM2. The capacity of each storage tank refers to the actual storage capacity, including not only the storage medium but also the tank shell and internal heat-transfer pipes. The thermal charging and discharging rate is denoted as $\dot{Q}$ with a unit of kW. Q represents the thermal charging and discharging amount of each thermal storage tank with a unit of kWh, and t denotes the thermal charging and discharging time in minutes.

$$\dot{Q} = \frac{Q}{t} \tag{11}$$

In this experiment, the sensors and measurement devices were configured as follows. A common outlet temperature sensor, $T_{PVT\ out}$, and individual outlet temperature sensors were installed for each thermal storage tank. Flow meters were installed near the outlet temperature sensors of each system. Data acquisition was performed using a Graphtec data logger. The outlet temperatures, flow rates, and internal temperature sensors of each thermal storage tank were recorded using the data logger.

2.3. Experimental period and operating conditions

This experiment was conducted from April 17 to June 30, 2025. The WTES used in the experiment had a capacity of 500 L, and the two prototype PCM-based thermal storage tanks had capacities of 11.51 L for PCM 1 and 7.71 L for PCM 2, both with shell-and-tube structures. When hot water at 50 °C and cold water at 25 °C were alternately supplied, the average thermal storage amount calculated from the inlet–outlet temperature difference of the thermal storage tanks was 1.164 MJ, and the thermal storage density was

161.52 MJ/m^3.

A charging–discharging cycle was applied, with thermal charging at 45 °C and thermal discharging at 20 °C, and the phase change temperature of the PCM was 39 °C. This value represents the characteristics of the PCM storage tank and does not mean that the inlet and outlet temperatures were controlled during the experiment.

Of the two prototype PCM-based thermal storage tanks, PCM 1 was an initial prototype, whereas PCM 2 was an improved version. This study analyzed the energy balance of KePSH-2 to identify the energy flow of each system. It evaluated the performance of prototype PCM-based thermal storage tanks by calculating the thermal storage capacity, thermal storage density, charging rate, and charging time for each tank. The thermal storage tanks used in the experiment are shown in Fig. 3. The internal design information of the prototype PCM-based storage tanks and the PCM properties are listed in Table 1.

2.4. Uncertainty analysis

This study conducted an uncertainty analysis of the PVT solar irradiance and thermal collection, as well as the thermal charging and discharging amounts of each thermal storage tank, to ensure experimental accuracy. The uncertainty analysis method proposed by Kline and McClintock (1953) was adopted [44]. Type An uncertainty (δ_{vr}), representing repeatability error, and Type B uncertainty

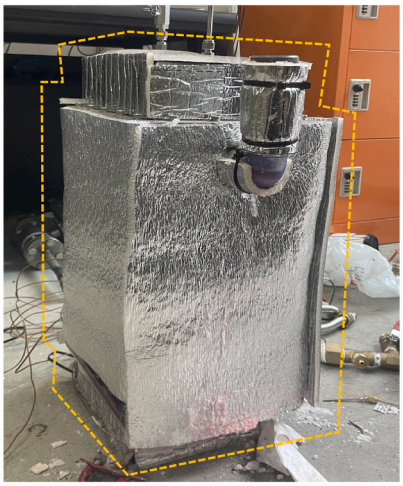

(a) Storage tank of PCM1

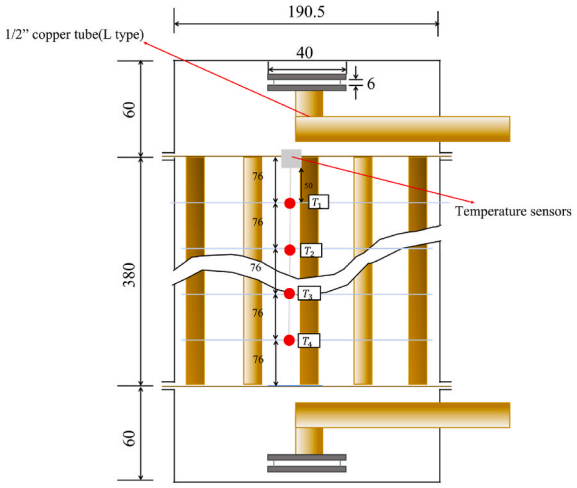

(c) Vertical cross-section of PCM1

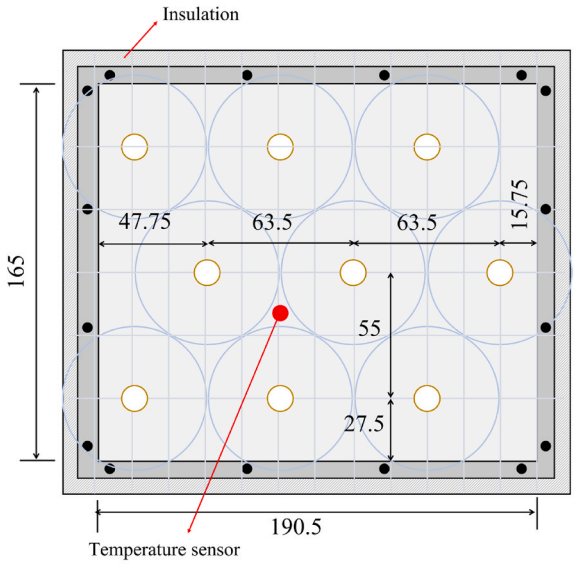

(b) Horizontal cross-section of PCM1

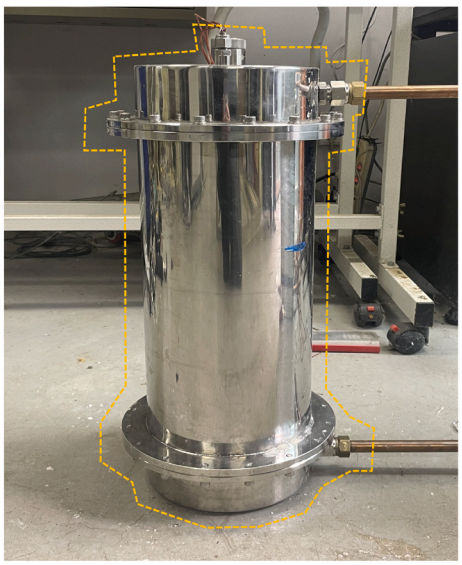

(d) Storage tank of PCM2

Fig. 3. Cross-section of PCM-based storages.

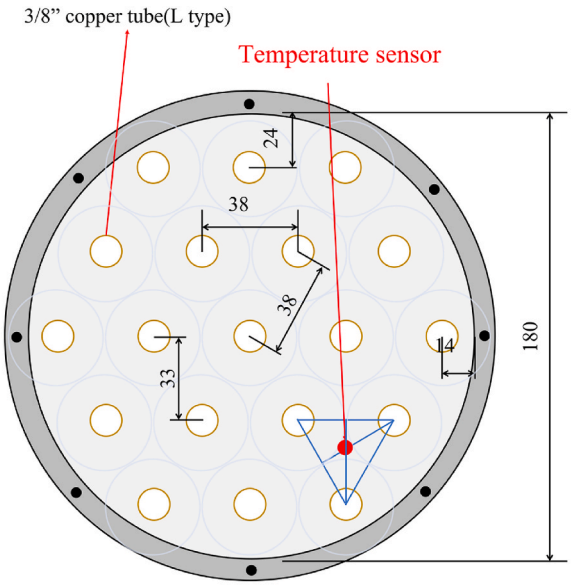

(e) Horizontal cross-section of PCM2

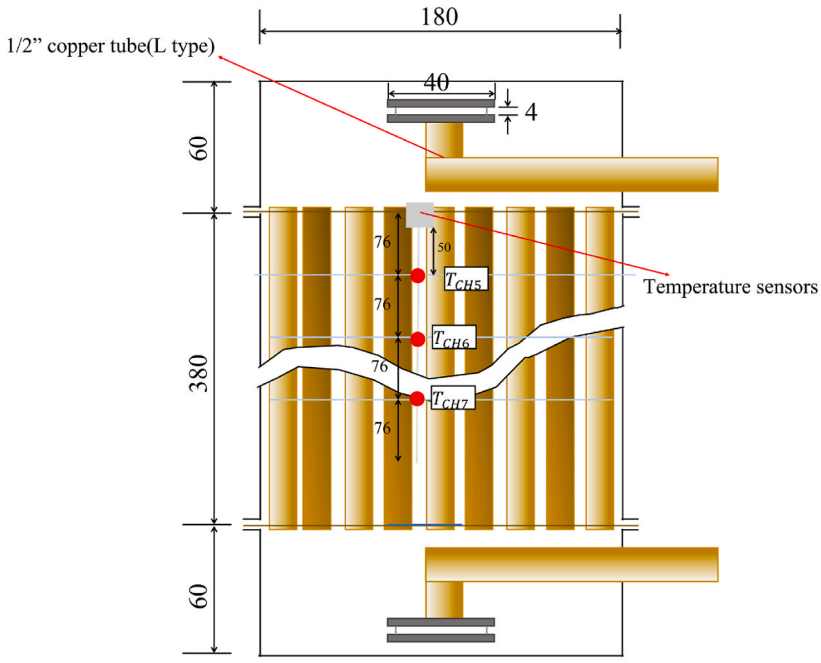

(f) Vertical cross-section of PCM2

Fig. 3. (*continued*).

(δ_{ve}), representing instrument error, were calculated for all experimental results, and the combined uncertainty (δ_v) was obtained by combining these two components. A Kipp & Zonen CMP 6 pyranometer was used to measure solar irradiance, with a measurement uncertainty of ±0.1%. The measurement uncertainty of the Toshiba LF620 flow meter was ±0.3%, and the measurement uncertainty of the OMEGA RTD 810, DIN A temperature sensor was ±0.1%. The standard deviation of solar irradiance (G) is denoted as σ_G. Equation (11) represents Type An uncertainty, Eq. (12) represents Type B uncertainty, and Eq. (13) represents the combined uncertainty.

Table 1
Specifications of PCM-based thermal storage tanks.

	PCM 1	PCM 2	Unit
Thermal Storage Tank Shape	Cuboid	Cylindrical	-
Cross-sectional Area	191 × 165	90 × 90	mm^2
Height	380	380	mm
Number of Copper Tubes	9	18	-
Copper Tube Type (L-Type)	10A (3/8″)	10A (3/8″)	-
Copper L-type Wall	0.89	0.89	mm
Copper L-type Outer Diameter	12.7	12.7	mm
Copper L-type Inner Diameter	10.92	10.92	mm
V	11.51	7.71	L
Pitch	63.5($5d_o$)	38($3d_o$)	mm
Volume Ratio of Tubes in Tank	3.6	10.1	%
Optimal Flow Rate of HTF (Heat-Transfer Fluid)	0.6 *Collector Area 0.5 m^2, 10 cm^3/s	0.4 *Collector Area 1 m^2, 1.2 LPM	LPM
Insulation Material	Closed-cell Elastomeric Foam	Closed-cell Elastomeric Foam	-
Insulation Thickness	13	13	T
Property of Paraffin Wax PCM	Values		Unit
Melting Temperature Range	29–36		°C
Melting Onset Temperature	30.3		°C
Melting Peak Temperature	35.8		°C
Latent Heat of Fusion	184.9		J/g
Package Size	230 × 180 × 25		mm
Attachment Method	Silicone, thermally conductive adhesive tape		-
Quantity	15		-

$$\delta_{vr_G} = \frac{\sigma_G}{\sqrt{N} \cdot \overline{G}} \times 100 \tag{11}$$

$$\delta_{ve_G} = 0.1 \tag{12}$$

$$\delta_{v_G} = \sqrt{\left(\delta_{vr_G}\right)^2 + \left(\delta_{ve_G}\right)^2} \tag{13}$$

The uncertainty analysis of the thermal charging amount for each system is described as follows. The standard deviation is denoted as σ_Q, where Eq. (14) represents the Type An uncertainty, Eq. (15) represents the Type B uncertainty, and Eq. (16) represents the combined uncertainty.

$$\delta_{vr_Q} = \frac{\sigma_Q}{\sqrt{N}} \times 100 \tag{14}$$

$$\delta_{ve_Q} = \sqrt{\left(\frac{\delta T}{T}\right)^2 + \left(\frac{\delta m}{m}\right)^2} \tag{15}$$

$$\delta_{v_Q} = \sqrt{\left(\delta_{vr_Q}\right)^2 + \left(\delta_{ve_Q}\right)^2} \tag{16}$$

The uncertainty analysis for the values calculated using the virtual sensors is as follows. The standard deviation is denoted as $\sigma_{m_{WTES}}$, where Eq. (17) represents the Type An uncertainty, Eq. (18) represents the Type B uncertainty, and Eq. (19) represents the combined uncertainty.

$$\delta_{vr_m_{WTES}} = \frac{\sigma_{m_{WTES}}}{\sqrt{N}} \times 100 \tag{17}$$

$$\delta_{ve_m_{WTES}} = \sqrt{(0.003)^2 + (0.003)^2 + (0.003)^2} \tag{18}$$

$$\delta_{v_m_{WTES}} = \sqrt{\left(\delta_{vr_m_{WTES}}\right)^2 + \left(\delta_{ve_m_{WTES}}\right)^2} \tag{19}$$

The standard deviation is denoted as $\sigma_{T_{WTES\ out}}$, where Eq. (20) represents the Type An uncertainty, Eq. (21) represents the Type B uncertainty, and Eq. (22) represents the combined uncertainty.

$$\delta_{vr_T_{WTES\ out}} = \frac{\sigma_{T_{WTES\ out}}}{\sqrt{N}} \times 100 \tag{20}$$

$$\delta_{ve_T_{WTES\ out}} = \sqrt{\left(\frac{\delta T}{T}\right)^2 + \left(\frac{\delta m}{m}\right)^2} \tag{21}$$

$$\delta_{v_T_{WTES\ out}} = \sqrt{\left(\delta_{vr_T_{WTES\ out}}\right)^2 + \left(\delta_{ve_T_{WTES\ out}}\right)^2} \tag{22}$$

The overall uncertainties of solar irradiance and the thermal charging amount of each system and each virtual sensor are expressed by Eqs. (23)–(26).

$$\delta_{v_G,RMS} = \sqrt{\frac{1}{N}\sum\left(\delta_{v_G}\right)^2} \tag{23}$$

$$\delta_{v_Q,RMS} = \sqrt{\frac{1}{N}\sum\left(\delta_{v_Q}\right)^2} \tag{24}$$

$$\delta_{v_Q,RMS} = \sqrt{\frac{1}{N}\sum\left(\delta_{v_m_{WTES}}\right)^2} \tag{25}$$

$$\delta_{v_Q,RMS} = \sqrt{\frac{1}{N}\sum\left(\delta_{v_T_{WTES\ out}}\right)^2} \tag{26}$$

The cumulative uncertainty analysis used in this study is expressed as follows.

The combined standard uncertainty of the heat quantity at each time step is given by Eq. (27), while the uncertainty of the cumulative energy corresponds to Eq. (28).

The uncertainty of the cumulative energy is obtained by integrating the instantaneous heat quantity over the experimental period, and the uncertainties at each time step are aggregated using the root sum square (RSS) method.

$$\frac{u(Q_i)}{\dot{Q}_i} = \sqrt{\left(\frac{u(\dot{m})}{\dot{m}}\right)^2 + \frac{u(T_{in})^2 + u(T_{out})^2}{(T_{out} - T_{in})^2}} \tag{27}$$

$$\boldsymbol{U}_{cum} = \sqrt{\sum\left(u(Q_i)\cdot\Delta t\right)^2} \tag{28}$$

$$\boldsymbol{U}_{rel,cum} = \frac{\boldsymbol{U}_{cum}}{\boldsymbol{E}_{total}} \times 100$$

The results of the uncertainty analysis are presented in Table 2.

Table 2
Uncertainty analysis.

RMS Uncertainty of Individual Data Points		
System Component		$\delta_{v_Q,RMS}$
-		%
G		0.43
$\boldsymbol{Q_{PVT}}$		3. 99
$\boldsymbol{Q_{WTES}}$		3.24
$\boldsymbol{Q_{PCM\ 1}}$		5.61
$\boldsymbol{Q_{PCM\ 2}}$		4.84
$\boldsymbol{Q_{HEX}}$		5.71
$\boldsymbol{T_{WTES\ out}}$		0.66
$\boldsymbol{m_{WTES}}$		0.85
Cumulative Energy Uncertainty		
System Component		$U_{rel,cum}$
Q_{WTES}	Charging	0.081
	Discharging	0.034
$Q_{PCM\ 1}$	Charging	0.087
	Discharging	0.169
$Q_{PCM\ 2}$	Charging	0.089
	Discharging	0.188

3. Experimental results

3.1. Thermal output profile of the vertical PVT system

Table 2 presents the daily solar irradiance, thermal collection amount, and collection efficiency of the vertical PVT system for each experimental date, as well as the thermal charging and discharging amounts of each thermal storage tank. The average thermal collection amount is 15.2 kWh, and the average collection efficiency is 39%. The maximum thermal collection amount is 26.4 kWh, and on the same date, the collection efficiency also reached the highest value of 52.9%.

The average thermal charging amount of the WTES is 9.4 kWh, whereas the prototype PCM-based thermal storage tanks show thermal charging amounts of 0.2 kWh for PCM1 and 0.4 kWh for PCM2. Considering that the average PVT thermal collection amount is 15.2 kWh, we can observe that 61.7% of the collected thermal energy is stored in the TES, 1.1% is stored in the prototype PCM1 thermal storage tank, and 2.4% is stored in the PCM2 thermal storage tank. In other words, the thermal storage amount of the TES is 57.6 times greater than that of PCM1 and 25.6 times greater than that of PCM2. This can be attributed to the larger capacity of the WTES, which is 500 L, compared to the prototype PCM-based thermal storage tanks with capacities of 11.51 L for PCM1 and 7.71 L for PCM2, meaning that the WTES has capacities 43.4 times and 64.9 times larger, respectively.

In this study, to analyze the effectiveness of the thermal storage tanks, a detailed analysis was conducted for the period from May 28 to May 31. Over these four days, the overall thermal collection efficiency ranged from a minimum of 30.4% to a maximum of 46.3%.

3.2. Charging and discharging behavior of each storage tank

The daily thermal charging and discharging amounts of each thermal storage tank are presented in Table 3. The average thermal charging amount of the WTES is 9.4 kWh/day. For the prototype PCM-based thermal storage tanks, the thermal charging amounts are 0.2 kWh/day for the PCM1 storage tank and 0.4 kWh/day for the PCM2 storage tank, and the thermal discharging amounts are 0.2 kWh/day for both storage tanks.

For the prototype PCM1-based thermal storage tank, the thermal discharging amount increased by 5.6% relative to the thermal charging amount. However, given that both the thermal charging and discharging amounts are 0.2 kWh/day, we can infer that most of the charged thermal energy was transferred to discharging. In the case of the PCM2-based thermal storage tank, the thermal discharging amount decreased by 57% relative to the thermal charging amount, indicating that approximately 43% of the stored thermal energy was released through discharging.

From the results of the thermal charging and discharging amounts of the prototype PCM1-based thermal storage tank, the 5.6% increase in discharging relative to charging could be interpreted as a violation of the law of energy conservation. However, because this experiment evaluated the performance of a latent heat thermal storage tank under actual PVT operating conditions, the inlet and outlet temperatures are not constant and vary depending on solar irradiance and PVT thermal collection. According to the uncertainty analysis of the calculated heat in this study, the uncertainties of prototype PCM1-based storage tank and prototype PCM2-based storage tank were 5.61% and 4.84%, respectively. This indicates that the overall uncertainty of the heat analysis in this experiment was approximately ±6%. Therefore, the result showing that the discharging amount of the prototype PCM1-based storage tank increased by approximately 5.6% compared to the charging amount can be interpreted as occurring within this experimental uncertainty range. In addition, when PCM stores thermal energy as a latent heat storage medium, the heat is not stored instantaneously, and a slight delay occurs. Therefore, the result showing a 5.6% higher discharging amount than charging amount for the prototype PCM1-based thermal storage tank can be attributed to the experimental conditions reflecting real PVT operation and the thermal storage delay characteristics of PCM. In particular, this experiment was conducted continuously throughout the entire experimental period from April 23 to June 11, 2025. During this process, the heat collected by the PVT on that day was reflected in the prototype PCM storage tank and appeared in the calculated values, but the heat accumulated inside the storage tank during the previous

Table 3
Daily experimental results.

Time	Q [kWh/day]		η_Q [%]	Charging [kWh/day]				Discharging [kWh/day]	
	G	Q_{PVT}		Q_{WTES}	Q_{PCM1}	Q_{PCM2}	Q_{HEX}	Q_{PCM1}	Q_{PCM2}
04-23-2025	37.1	16.2	43.7	10.7	0.2	0.5	4.4	0.2	0.1
04-30-2025	49.9	26.4	52.9	12.9	0.3	0.6	11.8	0.3	0.4
05-08-2025	37.1	16.2	43.7	10.7	0.2	0.5	4.4	0.2	0.1
05-12-2025	44.0	16.9	38.4	10.5	0.2	0.5	4.3	0.2	0.2
05-18-2025	42.1	15.9	37.8	5.8	0.1	0.3	4.3	0.2	0.1
05-02-2025	36.7	10.6	29.0	5.4	0.1	0.3	4.1	0.1	0.0
05-27-2025	39.7	19.0	47.7	16.3	0.2	0.3	7.9	0.2	0.2
05-29-2025	39.2	13.7	34.9	9.2	0.1	0.3	12.8	0.2	0.2
05-30-2025	40.0	18.5	46.3	10.4	0.1	0.3	8.0	0.1	0.1
05-31-2025	37.4	11.4	30.4	6.2	0.2	0.3	3.9	0.1	0.1
06-03-2025	37.1	11.3	30.4	6.7	0.1	0.3	4.0	0.1	0.1
06-05-2025	37.3	12.3	32.9	7.0	0.1	0.2	4.2	0.2	0.2
06-11-2025	33.7	12.7	37.8	8.2	0.1	0.2	4.1	0.3	0.2
Average	38.5	15.2	39.0	9.4	0.2	0.4	5.7	0.2	0.1

experimental period was not reflected. In addition, considering that the charging and discharging rate of the prototype PCM1-based storage tank was slow at 0.1 kW, a physical limitation in fully reflecting the daily PVT heat collection in the PCM storage tank exists.

The daily thermal flow of the thermal storage tanks was analyzed using the thermal charging and discharging data on May 30. The graphs of the PVT thermal collection, inlet and outlet temperatures, and flow rates of each thermal storage tank are shown in Fig. 4. The periods during which thermal charging occurs in the thermal storage tanks are indicated by the red regions in Fig. 4(a), whereas thermal discharging is indicated by the yellow regions. It is observed that thermal charging does not occur continuously during PVT operation, but rather during specific periods. According to the trend of the graph, thermal collection begins at 11:00 and continues until 15:00, which can be attributed to heat production by the operation of the solar thermal panels.

Among the thermal storage tanks, the WTES stores the largest amount of thermal energy, and the thermal charging and discharging periods of the WTES and PCM-based thermal storage tanks coincide. This can be confirmed by the identical red and yellow regions in Fig. 4(b)–4(d).

As shown in Fig. 4(e), it can be observed that the temporal patterns of the heat storage section of the geothermal heat exchanger (green region) and the heat release sections of each thermal storage tank (yellow region) overlap. It is also observed that the thermal energy released from the prototype PCM-based thermal storage tanks during discharging is supplied to the ground heat exchanger. In

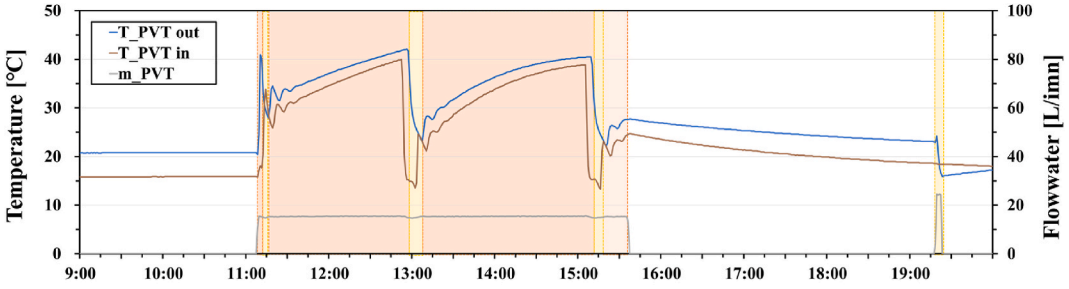

(a) PVT

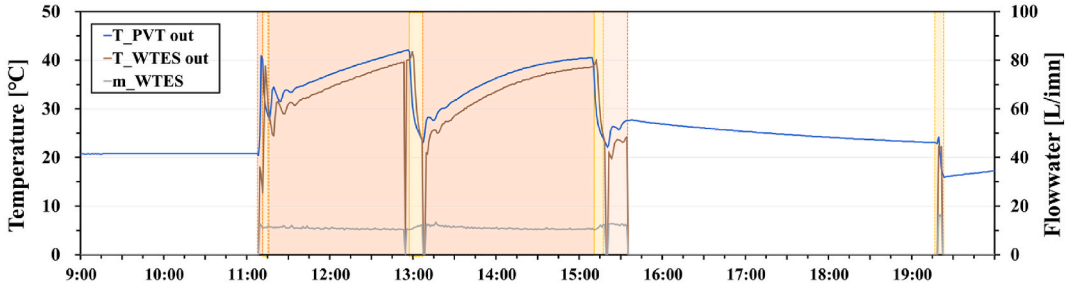

(b) WTES

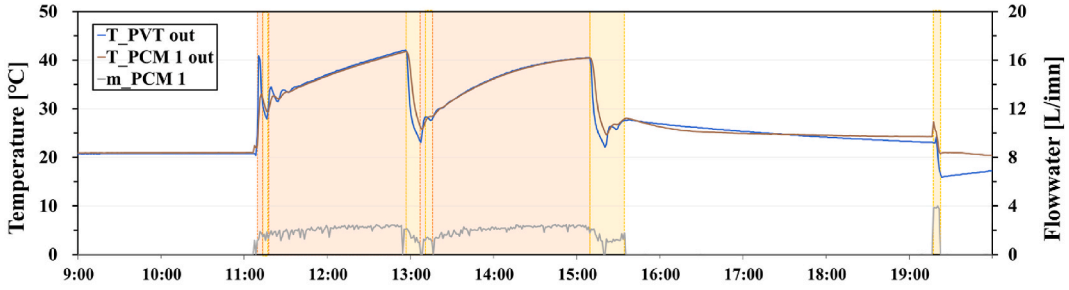

(c) PCM1

Fig. 4. Inlet and outlet temperatures and flow rate.

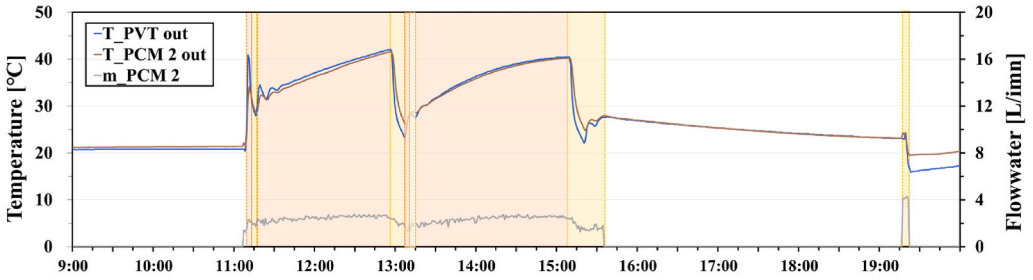

(d) PCM2

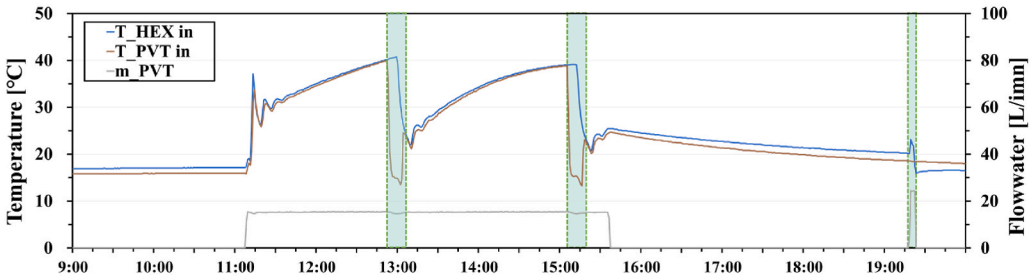

(e) HEX

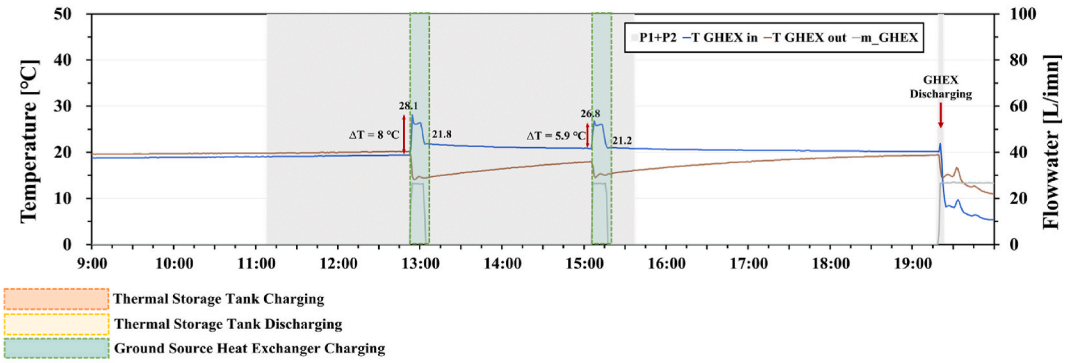

(f) GHEX

Fig. 4. (*continued*).

addition, the discharging period of the prototype PCM-based thermal storage tanks occurs first, followed by the period during which thermal energy is supplied to the ground. This suggests that thermal discharging from the prototype PCM storage tanks occurs first, and thermal energy is subsequently supplied to the ground heat exchanger.

Fig. 4 shows the short periods during which the inlet and outlet temperatures decrease simultaneously. Around these periods, thermal charging occurs in the regions marked in yellow, followed by thermal discharging in the regions marked in green. Furthermore, the thermal energy flowing to the ground occurs immediately after the discharging of yellow regions corresponding to prototype PCM-based thermal storage. However, the green regions representing heat transfer to the ground and the yellow regions show similar trends, indicating that the PCM discharging and ground heat charging occur during the same time periods.

Additionally, the behavior of each thermal storage tank exhibits a similar pattern in response to variations in the PVT outlet temperature. Prior to PVT heat collection (before 11:08), the PVT temperature remains at approximately 20 °C, and increases up to a maximum of 42.1 °C after the onset of heat collection. This period, from 11:09 to 13:00, corresponds to the first heat collection interval. During the same interval, the outlet temperature of the WTES also increases from 18 °C to 40 °C, indicating that heat storage occurs simultaneously with PVT heat collection. In the case of the PCM thermal storage tanks, prior to heat collection, PCM 1 and PCM

2 maintain temperatures of 21 °C and 21.4 °C, respectively. During the collection period, the outlet temperature of PCM 1 increases from 27.8 °C to a maximum of 41.7 °C, while PCM 2 shows an increase from 31.3 °C to 41.6 °C. In other words, although the outlet temperature of the WTES increases by 22 °C (from 18 °C to 40 °C), the PCM-based storage tanks exhibit smaller temperature rises of 13.9 °C for PCM 1 and 10.3 °C for PCM 2 over the same interval.

Even within the same PVT heat collection period, it can be observed that the outlet temperature difference (Δ T) of the WTES is greater than that of the PCM-based storage tanks.

These results indicate that the outlet temperatures of all thermal storage tanks vary in accordance with the behavior of the PVT system.

As shown in Fig. 4(f), which illustrates the behavior of the GHEX, the inlet temperature of the GHEX increased to 28.1 °C around 13:00 due to the heat transferred from the thermal storage tank, and then decreased to 21.8 °C after the charging process ended. This indicates that the heat stored in the tank was transferred to the ground heat exchanger, resulting in an approximately 8 °C increase in the ground-side temperature. A similar trend was also observed during the second charging period around 15:30, when the inlet temperature of the GHEX increased again.

Therefore, the daily charging and discharging thermal energy amounts presented in this study should be interpreted as indicators characterizing the intrinsic thermal behavior of PCM. Rather, as energy balance indicators for evaluating the thermal energy flow charged into and discharged from each thermal storage tank under actual PVT operating conditions. Since the heat source of the thermal storage tanks is the thermal energy collected by the PVT system, this analysis is specifically designed for the experimental PVT with PCM thermal storage system. In particular, because PCM exhibits thermal delay during both charging and discharging throughout the phase change process, the daily charging and discharging amounts alone are insufficient to fully describe the characteristics of PCM.

3.3. Comparison of thermal storage capacities (water vs PCM tanks)

Table 4 presents the daily thermal charging and discharging density, charging rate, charging time, discharging rate, and discharging time for each experimental date. The average thermal charging density of the WTES is 18.7 kWh/m^3, whereas those of the PCM1 and PCM2 thermal storage tanks are 14.1 kWh/m^3 and 47.4 kWh/m^3, respectively. The prototype PCM-based thermal storage tanks exhibit higher thermal storage density than the WTES. Because the actual volumes of the storage tanks used in this study were different, a limitation exists in directly comparing the absolute reduction in installation area. When the storage density was converted based on the same stored heat amount, the PCM2-based storage tank could store the same amount of heat with only 39.4% of the volume compared with the WTES. This indicates a reduction of more than 60% in storage tank installation space. This result can be attributed to the use of latent heat in the PCM2-based thermal storage tank, which enables higher energy density than water at the same volume.

The thermal charging rate of the WTES is 2.6 kW, whereas the charging rates of the PCM1 and PCM2 thermal storage tanks are both 0.1 kW. Therefore, the thermal charging rate of the WTES is 97.6% higher than that of the PCM1 storage tank and 95.7% higher than that of the PCM2 storage tank. This can be explained by the reduced heat-transfer rate of prototype PCM-based thermal storage tanks during the phase change process owing to the use of latent heat. The thermal charging times are 217.9 min for the WTES, 155.4 min for PCM1, and 195.8 min for PCM2. The prototype PCM1-based thermal storage tank has the shortest charging time, and the difference in charging times between the longest (i.e., WTES) and the shortest (i.e., PCM1-based thermal storage tank) is 62.5 min. Although the prototype PCM-based thermal storage tanks have similar charging times ranging from 155.4 to 195.8 min, they exhibit higher thermal storage density, resulting in greater energy storage per unit volume. However, owing to their lower charging rates, certain limitations exist in rapid TES.

The thermal discharging performance of the prototype PCM-based thermal storage tanks is as follows. The thermal discharging densities are 14.9 kWh/m^3 for PCM1 and 20.4 kWh/m^3 for PCM2. For the PCM1 storage tank, the discharging density increased by 5.6% compared to the charging density, indicating that the prototype PCM1-based thermal storage tank exhibits similar performance in terms of charging and discharging density. In contrast, the prototype PCM2-based thermal storage tank shows a 57% reduction in discharging density compared to the charging density, indicating that higher energy density is achieved during the charging process than during discharging. The thermal discharging rates are 0.3 kW for both the PCM1-and PCM2-based thermal storage tanks. Given that the charging rates of both storage tanks were 0.1 kW, the discharging rates increased by 301.3% for the PCM1 storage tank and by 127.8% for the PCM2 storage tank compared to the charging rates. This indicates that both PCM-based thermal storage tanks exhibit faster discharging rates than charging rates. The thermal discharging times are 40.9 min for the prototype PCM1-based thermal storage tank and 37.0 min for the prototype PCM2-based thermal storage tank, indicating that both prototype PCM-based thermal storage tanks have similar discharging times exceeding 35 min.

3.4. Effectiveness of each storage configuration as a buffer

A portion of the thermal energy stored in the thermal storage tanks is supplied to the ground heat exchanger and discharged. Table 3 lists the thermal discharging from the prototype PCM-based thermal storage tanks and the thermal energy supplied to the ground. The average thermal discharging amount of the prototype PCM-based thermal storage tanks is 0.2 kWh for the prototype PCM1-based storage tank and 0.2 kWh for the prototype PCM2-based storage tank, resulting in an average total discharging amount of 0.3 kWh for the two prototype PCM-based thermal storage tanks. The thermal energy supplied to the ground is 5.7 kWh. In this experiment, only the thermal discharging amount of the prototype PCM-based thermal storage tanks was considered; therefore, the

Table 4
Charging and discharging densities and thermal rates of each storage.

Time	Charging									Discharging					
	ρ [kWh/m^3]			$\dot{Q}$ [kW]			Duration [min]			ρ [kWh/m^3]		$\dot{Q}$ [kW]		Duration [min]	
	WTES	PCM1	PCM2	WTES	PCM1	PCM2	WTES	PCM1	PCM2	PCM1	PCM2	PCM1	PCM2	PCM1	PCM2
04-23-2025	21.4	17.7	64.4	2.3	0.1	0.1	273.0	169.0	258.0	18.9	19.0	0.2	0.3	53	29.0
04-30-2025	25.9	27.9	79.8	2.3	0.1	0.1	343.0	271.0	309.0	27.5	45.6	0.3	0.3	69	66.0
05-08-2025	21.4	17.7	64.4	2.3	0.1	0.1	273.0	169.0	258.0	18.9	19.0	0.2	0.3	53	29.0
05-12-2025	21.0	16.1	60.2	2.0	0.0	0.1	309.0	240.0	294.0	13.7	20.0	0.3	0.3	31	27.0
05-18-2025	18.7	12.3	48.8	2.2	0.0	0.1	254.0	179.0	237.0	14.1	18.8	0.3	0.3	29	29.0
05-21-2025	11.6	12.7	35.8	2.5	0.1	0.1	140.0	105.0	114.0	13.7	19.1	0.3	0.3	36	35.0
05-27-2025	18.4	13.8	48.3	2.2	0.1	0.1	246.0	175.0	215.0	19.3	32.0	0.3	0.3	44	57.0
05-29-2025	25.2	20.2	50.6	4.2	0.1	0.1	182.0	146.0	163.0	18.6	26.7	0.3	0.3	50	41.0
05-30-2025	18.4	8.7	38.9	2.3	0.0	0.1	241.0	173.0	210.0	17.4	25.9	0.3	0.2	47	52.0
05-31-2025	20.8	8.7	42.8	4.4	0.1	0.1	143.0	116.0	133.0	12.6	13.0	0.3	0.2	34	30.0
06-03-2025	12.3	13.2	39.4	2.5	0.1	0.2	146.0	100.0	121.0	10.5	17.4	0.2	0.2	37	34.0
06-05-2025	13.4	12.1	37.0	2.5	0.1	0.1	164.0	104.0	143.0	10.1	18.3	0.2	0.3	29	32.0
06-11-2025	14.0	9.9	26.3	2.4	0.1	0.1	174.0	75.0	138.0	13.7	20.0	0.2	0.3	50	37.0
Average	18.7	14.1	47.4	2.6	0.1	0.1	217.9	155.4	195.8	14.9	20.4	0.3	0.3	40.9	37.0

thermal energy supplied to the ground heat exchanger exceeds the thermal energy discharged from the storage tanks. However, by additionally considering the discharging amount of the WTES and the heat losses in the piping within the experimental environment, the thermal energy transferred in each system can be more accurately quantified.

Table 5 presents the time-resolved heat storage and release rates of each thermal storage tank on May 30. If the daily energy balance presented above is used to evaluate the overall thermal energy flow of the PVT with thermal storage system, the charging and discharging rates presented in Table 5 serve as indicators for the thermal delay characteristics of the PCM thermal storage tanks. During the PVT operation period, the WTES and prototype PCM-based storage tanks exhibit alternating heat storage and release behavior.

Furthermore, the results clearly demonstrate the significantly slower heat storage and release rates of the prototype PCM-based storage tanks. The average heat storage rate of the WTES reaches 2.6 kW, with a peak heat transfer rate of 6.7 kW observed during a specific interval (i.e., 11:07–11:13). In contrast, the average heat storage rates of PCM 1 and PCM 2 are approximately 0.02 kW and 0.1 kW, respectively, indicating substantially limited heat absorption performance compared to the WTES.

This quantitatively suggests that, due to the low thermal conductivity of phase change materials and the thermal lag associated with the phase change process, the prototype PCM-based storage tanks are unable to sufficiently accommodate the heat generated by the PVT system in real time.

A similar trend is observed in the heat release behavior. While the WTES exhibits an average heat release rate of 1.5 kW, PCM 1 and PCM 2 show lower release rates of 0.5 kW and 0.3 kW, respectively. In particular, the PCM-based storage tanks exhibit characteristics of releasing heat at relatively low rates over longer durations compared to the WTES during specific intervals (i.e., 12:54–13:18, 15:12–15:35, and 19:17–19:21).

In conclusion, although the PCM 2 storage tank has a higher energy density than the WTES, its slower heat storage and release rates indicate that optimization of the internal heat transfer structure is essential for real-time load response under dynamically varying heat source conditions, such as actual PVT operation.

Such dynamic behavior can be attributed to the characteristics of phase change materials, in which thermal charging and discharging do not occur instantaneously, and the heat-transfer rate is relatively slow. In other words, a thermal-transfer delay effect of PCM can be identified. The internal temperatures of the PCM-based thermal storage tanks are shown in Fig. 5. The latent heat regions observed in Fig. 5 are periods during which the internal temperature of the storage tank remained temporarily constant. This indicates that the heat transferred during the charging and discharging of the PCM1 storage tank corresponded to the latent heat region associated with the phase change process. In the latent heat 1 region, this is interpreted as the release of heat stored on the previous day in the form of latent heat. Additionally, regions where the temperature increased or decreased are interpreted as sensible heat regions, where heat is stored and released. Furthermore, heat collected from the PVT entered the upper part of the PCM-based storage tank. The temperatures T1 and T2 at the upper part of the PCM1 storage tank were up to 2 °C higher than T3 and T4 at the lower part. This indicates that the internal stratification of the storage tank was not caused by the high outlet temperature of the PVT.

3.5. Contribution of each storage tank to enhancing PVT heat utilization

Under actual PVT operating conditions, a comparison of the thermal energy of each system showed that, of the 15.2 kWh collected by the PVT system, 61.7% (9.4 kWh) was stored in the WTES. The remaining thermal energy was stored in the prototype PCM-based thermal storage tanks, with 0.2 kWh and 0.4 kWh stored in each tank. In other words, 1.1% and 2.4% of the collected thermal energy were stored in the respective PCM thermal storage tanks. In terms of the thermal charging amounts stored in each thermal storage tank, more than half of the collected thermal energy was transferred to the WTES, attributable to its large capacity of 500 L.

Therefore, when comparing the thermal charging amounts on a unit-volume basis using thermal storage density, the WTES showed

Table 5
Time series analysis of thermal charging and discharging rates.

Time	min	WTES	PCM 1	PCM 2
0:00–11:06	660	0	0	0
11:07–11:13	7	6.7	0.30	0.34
11:14–11:15	2	−2.9	−0.16	−0.08
11:16–12:53	98	2.0	0.05	0.12
12:54–13:03	10	−2.7	−0.39	−0.40
13:04–13:18	15	2.3	−0.05	−0.15
13:19–14:23	65	2.2	0.02	0.05
14:24–15:05	42	1.6	0.01	0.06
15:06–15:11	6	0.2	−0.20	−0.17
15:12–15:16	5	−4.7	−0.70	−0.60
15:17–15:35	19	2.3	−0.05	−0.12
15:36–19:16	221	0	0	0
19:17	1	0.0	−1.15	−0.38
19:18–19:20	3	0.3	−0.58	−0.23
19:21	1	−5.4	−0.92	−0.65
19:22–23:59	277	0	0	0
Charging $\dot{Q}$ [kW]	-	2.6	0.02	0.1
Discharging $\dot{Q}$ [kW]	-	1.5	0.5	0.3

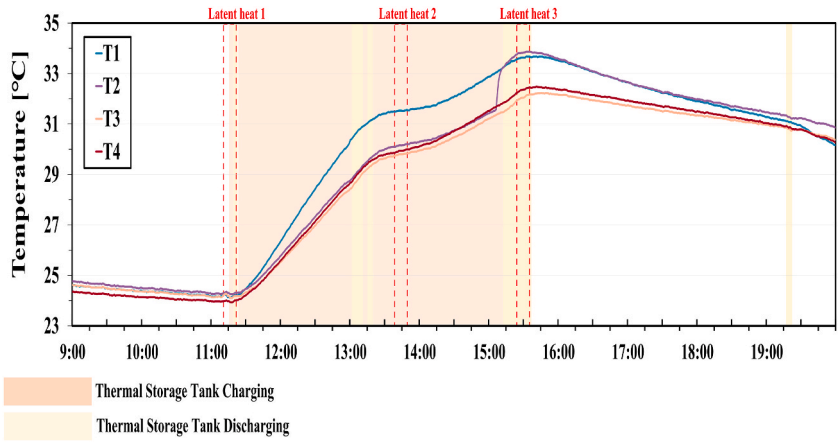

Fig. 5. Inner temperature of PCM1.

18.7 kWh/m^3, the prototype PCM1-based thermal storage tank showed 14.1 kWh/m^3, and the prototype PCM2-based thermal storage tank showed 47.4 kWh/m^3. This indicates that, for the same volume, the prototype PCM2-based thermal storage tank can store more thermal energy than the WTES. In other words, if the prototype PCM2-based thermal storage tank is scaled to the same capacity as the WTES and integrated into a PVT system, more thermal energy can be stored in a smaller space. Installing one PCM2-based thermal storage tank can provide a thermal storage amount equivalent to installing 2.5 times as many WTES.

However, the prototype PCM1-based thermal storage tank exhibited a lower thermal storage density than the WTES, likely because of its internal design. Although the two prototype PCM thermal storage tanks used the same latent heat material, differences exist in the piping configuration and capacity. Compared to the prototype PCM1-based thermal storage tank, the prototype PCM2-based thermal storage tank had a 72% reduction in cross-sectional area, and the number of heat-transfer pipes increased from 9 to 18 3/8-inch pipes. In addition, the spacing between pipes was reduced from 63.5 mm to 38 mm, improving the internal design to facilitate heat transfer. The ratio of pipe area to total storage tank capacity was 3.6% for PCM1 and 10.1% for PCM2. Thus, a higher thermal storage density could be achieved through a more efficient internal design, which enables the working fluid to pass through a larger number of pipes and enhances heat transfer. In this study, the real-time heat storage and release behavior was analyzed at a 1-min resolution under actual PVT operating conditions with dynamically varying thermal loads. In the case of the initial prototype (PCM 1), the pipe pitch ranged from 15.75 to 63.5 mm, whereas the improved design (PCM 2) reduced the pitch to 14–38 mm. This design modification alleviated the thermal load per individual pipe by reducing the effective heat transfer burden, thereby compensating for the inherently slow heat storage characteristics of PCM. As a result, both the heat storage density and the charging rate were simultaneously enhanced. In terms of the thermal charging rate, limitations arise owing to the latent heat storage characteristics of PCM thermal storage tanks.

For the WTES, the charging rate is 2.6 kW, corresponding to 26 kJ of heat storage per minute. In contrast, the charging rate of the prototype PCM-based thermal storage tanks is 0.1 kW, corresponding to 1 kJ of heat storage per minute. The discharging rate of the prototype PCM-based thermal storage tanks is 0.3 kW, approximately three times the charging rate; however, it is still slower than that of the WTES. This is because prototype PCM-based thermal storage tanks store thermal energy through a solid-to-liquid phase change during charging, and heat transfer is slower owing to the low thermal conductivity of the solid phase. Under actual PVT operating conditions, this slow charging and discharging rate of PCM can be a limitation, as it may not allow thermal energy to be stored and released in real time.

This study compared the thermal storage performance of the WTES and the prototype PCM1-based thermal storage tank. The experimental results obtained from the prototype PCM1-based tank showed that the thermal storage performance of the PCM-based tank was affected by internal design factors, particularly the heat transfer area. The results also showed that, in this experimental case, when the heat transfer area was not sufficiently considered, the high heat capacity of the PCM was not effectively utilized and thermal delay occurred during the charging process. To address this limitation, the prototype PCM2-based storage tank increased the number of pipes and reduced the pipe spacing to increase the heat-transfer area. This reduced the thermal delay characteristic of PCM and maximized the latent heat storage capability, and the prototype PCM2-based storage tank showed higher thermal charging and discharging densities than the prototype PCM1-based storage tank. The scope of this study focuses on the thermal storage performance analysis of the storage tanks.

A conventional 500 L WTES imposes a load of approximately 0.5 tons, making indoor installation within residential units challenging. To address these limitations, the prototype PCM-based thermal storage tank developed in this study achieved a high thermal energy density per unit volume by utilizing latent heat, thereby demonstrating considerable potential for system downsizing. This suggests that the proposed system can serve not only as an improvement in performance but also as a practical alternative for indoor installation in apartment buildings.

3.6. Discussion

This study installed thermal storage tanks under long-term, real-world PVT operating conditions, enabling observation of thermal charging and discharging behavior under dynamically varying thermal input. Most previous studies have evaluated the performance of PCM-based thermal storage tanks under constant inlet temperature and flow rate conditions in controlled laboratory environments. In contrast, the present work assessed the responsiveness of prototype PCM tanks dynamically varying heat input under actual PVT coupled operation. Since PVT systems generate thermal energy that fluctuates with real-time solar irradiance, the effectiveness of a connected storage tank depends on its capability to store excess heat during the day and supply it when required to meet nighttime demands.

The charging and discharging rates measured under actual PVT operation (Table 5) show that both PCM-based prototype tanks are too slow to function as thermal buffers under real PVT operating conditions, even though the PCM2 prototype has a higher storage density than the WTES reference. This slow dynamic response is the main practical limitation of the PCM-based thermal storage tanks tested in this study. The dynamic behavior was not quantified using indicators such as response time, thermal delay, and load-following capability, which is a limitation of this analysis.

The WTES used in this experiment had a capacity of 500 L, whereas the PCM-based storage tanks had capacities of 7.71 L and 11.51 L. The WTES capacity was therefore approximately 43.4 to 64.9 times larger than that of the PCM-based storage tanks. Because of this large difference in storage capacity, the absolute charging and discharging amounts of the WTES and the PCM-based tanks are not compared directly. The WTES is used as a system-level reference rather than as a technical benchmark for the PCM tanks. Accordingly, the performance of each storage tank is evaluated using the thermal storage density, defined as the amount of stored or released heat per unit volume. This indicator allows storage tanks of different volumes to be compared on a common basis and reflects the feasibility of installation in constrained residential spaces, where the available footprint.

Within this comparative framework, the results suggest that the thermal storage behavior of a PCM-based tank is governed not only by the thermophysical properties of the PCM but also by the internal heat transfer structure. The internal pipe pitch is a key parameter determining heat transfer efficiency. In the initial PCM1 model, the pipe pitch ranged from a minimum of 15.75 mm to a maximum of 63.5 mm, resulting in a relatively large thermal influence radius of PCM assigned to each individual pipe. In contrast, the second PCM2 prototype was designed with a reduced pitch of 14 to 38 mm and an increased number of pipes. This reduction in pitch decreases the internal thermal resistance of the PCM and increases the effective heat transfer area, thereby enabling enhanced heat storage and release rates compared with PCM1. The two prototypes also differed in tank geometry, with PCM1 being rectangular and PCM2 being cylindrical, which may have additionally contributed to differences in effective PCM volume and internal heat transfer characteristics. These observations indicate that the internal piping configuration and tank geometry can influence the thermal storage behavior of PCM-based tanks. This is a component-level finding rather than a general design conclusion.

The daily energy balance analysis used in this study was adopted to evaluate the thermal energy flow under actual PVT operating conditions. However, because PCM does not store and release thermal energy instantaneously during the phase change process and instead exhibits thermal delay, the daily charging and discharging amounts alone have limitations in fully interpreting the intrinsic dynamic thermal behavior of PCM thermal storage tanks. Therefore, this study additionally presents the charging and discharging rates for each time interval in Table 5, which were used as complementary indicators for interpreting the dynamic thermal characteristics of the PCM thermal storage tanks. Several limitations of the component level analytical scope should be acknowledged. First, the absorbed and released heat was not decomposed into latent and sensible components, which restricts the depth of interpretation regarding the phase change contribution. Second, detailed measurements of the wall temperature of the installation space, as well as the thermal delay and thermal response time of the storage tanks, were not obtained, which constrained a more in depth analysis of the charging and discharging behavior of the PCM. Third, because the experimental period was limited to approximately two months between April and June at a single site in Daejeon, Republic of Korea, seasonal operating characteristics, long term reliability, and thermal aging of the PCM under repeated phase change cycles could not be evaluated. Despite these limitations, the occurrence of the phase change phenomenon could be indirectly identified from the temperature plateau observed in the internal temperature profile of

Table 6
Comparison of PCM storage performance with previous studies.

Reference	PCM type/melting point	Storage Capacity (Volume)	Conditions	Key Improvement (vs WTES)
Joseph et al. (2016) [28]	PureTemp 53 (Bio-based)/53 °C	60 L	Charge inlet 65 °C Discharge inlet 20 °C	+20% increase in storage capacity
Teamah et al. (2018) [29]	Cascaded Paraffins/48 °C, 54 °C, 60 °C	75 L(PCM) 630L(WTES)	Flow 1.5-3L/min	50% reduction in tank volume
Zhao et al. (2018) [30]	Salt Hydrates ($Na_2S_2O_3$, 5 H_2O)/35.5 °C	147 L	inlet 30-50 °C	20% reduction in tank volume
Koželj et al. (2021) [31]	Paraffin (RT44HC)/42–44 °C	800 L	Flow 0.083 kg/s Charge inlet 55 °C	70% increase in storage capacity
Huang et al. (2025) [24]	Paraffin (RT50)/45–51 °C	150 L	Flow 6-12 L/min Charge inlet 65 °C	30% increase in charge/discharge
This study	Paraffin Wax/29–36 °C	7.71L (PCM 1) 11.51 L(PCM 2), (vs 500L WTES)	PVT system	PCM 1: - 24.6% PCM 2: +153.4% In energy density (vs WTES)

the PCM1 storage tank. Additional experiments are planned to investigate seasonal performance variations, particularly under low solar irradiance conditions such as winter, and an extended study incorporating both the intrinsic thermal characteristics of the PCM and the specific installation environment of the PVT system is currently being prepared.

A further limitation of this study is that detailed system level performance data, such as the coefficient of performance of the heat pump and the temperature behavior of the heat exchanger during heat release from each thermal storage tank toward the ground heat exchanger, were not presented. A quantitative evaluation of the resulting impact on the heat pump performance and the ground heat exchanger operation lies beyond the present scope, and the related system level aspects have been examined in our previous work [41]. Experiments integrating the heat pump with the thermal storage tank operating as a buffer system are currently underway to evaluate the heat pump performance under coupled operation, and the results will be reported in a future publication. A dedicated building level performance assessment, integrating the present component level findings with the system level metrics, is planned as a follow up study.

In this study, as shown in Table 6, a quantitative benchmark of the measured charging and discharging densities against published values for alternative TES technologies under comparable operating regimes was included. However, the charging and discharging rates measured under actual PVT operating conditions not only provide a benchmark for future improvements in PCM thermal storage tank design, but also demonstrate the applicability of PCM thermal storage tanks under practical operating conditions. The main finding of this study is that both prototype PCM thermal storage tanks exhibited lower charging and discharging rates than the WTES, confirming that their dynamic thermal response was insufficient for use as real-time thermal buffer tanks in actual PVT systems. In particular, the results presented in Table 5 suggest that, for the practical application of PCM thermal storage tanks, improving the internal heat-transfer structure is essential not only to achieve high thermal storage density but also to simultaneously enhance the charging and discharging rates. Future studies should accordingly scale up PCM storage tanks to capacities comparable to those of conventional water tanks, conduct comparative experiments under matched operating conditions, and develop internal designs optimized for larger capacities to reduce thermal delay while maximizing the latent heat storage capability.

4. Conclusions

The performance of water- and prototype PCM-based thermal storage tanks was compared under actual PVT operating conditions. The average thermal collection of the PVT system was 15.2 kWh, of which 9.4 kWh was transferred to the WTES, whereas 0.2 kWh and 0.4 kWh were stored in the prototype PCM1-based and prototype PCM2-based thermal storage tanks, respectively. The thermal storage density, which represents the performance of the thermal storage tanks, was 18.7 kWh/m^3 for the WTES, 14.1 kWh/m^3 for the prototype PCM1-based thermal storage tank, and 47.4 kWh/m^3 for the prototype PCM2-based thermal storage tank.

Under actual PVT operating conditions, the prototype PCM-based tanks showed charging rates of 0.1 kW, compared to 2.6 kW for the WTES. This indicates that the prototype PCM-based tanks are insufficient to function as real-time thermal buffers in a PVT-coupled building system. This slow dynamic response is the main limitation of the prototype PCM tanks. Although prototype PCM2 exhibited a higher thermal storage density than prototype PCM1, the results of this study demonstrate that high thermal storage density alone is insufficient to achieve the dynamic thermal response required under actual PVT operating conditions. In this study, water- and prototype PCM-based thermal storage tanks were installed under actual PVT operating conditions, and the performance of each storage tank was analyzed. However, thermal storage tanks with different volumes were installed, with the WTES having a capacity of 500 L and prototype PCM-based thermal storage tanks, each with a capacity of 7.71 L. Owing to this volume difference, more than 50% of the PVT thermal collection was transferred to the WTES. If thermal storage tanks with the same capacity had been installed, the latent heat storage characteristics of PCM could have been observed more clearly. In addition, certain limitations exist in estimating the thermal discharging amount of the WTES. Because the outlet temperature and flow rate of the WTES were assumed to be virtual sensor values, comparing the thermal charging and discharging amounts of the WTES was difficult. Therefore, this study should be regarded as a field case study evaluating the thermal behavior of two prototype PCM thermal storage tanks under actual PVT operating conditions, and it has limitations in being generalized as a comprehensive demonstration of system-level application performance in buildings. Although the experimental results provide quantitative observations showing that the internal configuration can affect the behavior of PCM-based thermal storage tanks, the PCM2-based tank developed in this study is not intended to present a definitive design standard for PCM-based thermal storage systems. Therefore, in future studies, by considering accurate thermal energy values that exclude heat losses within the piping and transient thermal energy caused by temporary temperature differences between pipes, the discharging performance of the WTES can also be analyzed. Therefore, future studies should focus on improving the internal heat-transfer structure to maintain the high thermal storage density of PCM while achieving charging and discharging rates comparable to those of conventional WTES.

CRediT authorship contribution statement

Ye-Bin Shin: Data curation, Formal analysis, Writing – original draft. **Deuk-Won Kim:** Methodology, Resources, Validation. **Wangje Lee:** Investigation, Software. **Jae-Weon Jeong:** Supervision, Writing – review & editing. **Min-Hwi Kim:** Funding acquisition, Project administration, Supervision.

Declaration of competing interest

The authors declare that they have no known competing financial interests or personal relationships that could have appeared to

influence the work reported in this paper.

Acknowledgement

This work is supported by the Korea Agency for Infrastructure Technology Advancement (KAIA) grant funded by the Ministry of Land, Infrastructure and Transport (Grant RS-2025-02316198) and funded by the Korea Institute of Energy Research's (KIER's) Basic Project (grant number C6-2410-32).

Data availability

The data that has been used is confidential.

References

[1] L. Chen, Y. Hu, R. Wang, X. Li, Z. Chen, J. Hua, A.I. Osman, M. Farghali, L. Huang, J. Li, L. Dong, D.W. Rooney, P.-S. Yap, Green building practices to integrate renewable energy in the construction sector: a review, Environ. Chem. Lett. 22 (2024) 751–784, https://doi.org/10.1007/s10311-023-01675-2.
[2] A. Behzadi, A. Arabkoohsar, Y. Yang, Optimization and dynamic techno-economic analysis of a novel PVT-based smart building energy system, Appl. Therm. Eng. 181 (2020) 115926, https://doi.org/10.1016/j.applthermaleng.2020.115926.
[3] T. Ma, M. Li, A. Kazemian, Photovoltaic thermal module and solar thermal collector connected in series to produce electricity and high-grade heat simultaneously, Appl. Energy 261 (2020) 114380, https://doi.org/10.1016/j.apenergy.2019.114380.
[4] A. Miglioli, N. Aste, C. Del Pero, F. Leonforte, Photovoltaic-thermal solar-assisted heat pump systems for building applications: integration and design methods, Energy Built Environ. 4 (1) (2023) 39–56, https://doi.org/10.1016/j.enbenv.2021.07.002.
[5] F. Selimefendigil, C. Şirin, Energy and exergy analysis of a hybrid photovoltaic/thermal-air collector modified with nano-enhanced latent heat thermal energy storage unit, J. Energy Storage 45 (2022) 103467, https://doi.org/10.1016/j.est.2021.103467.
[6] A. Vallati, C.V. Fiorini, G. Lo Basso, F. Muzi, P. Oclon, M. Di Matteo, Optimization of a thermal storage tank for a water–water heat pump solar assisted system, Proc. 8th Int. Conf. Smart Sustain. Technol. (SpliTech) (2023) 1–7, https://doi.org/10.23919/SpliTech58164.2023.10192989.
[7] G. Gan, Y. Xiang, Experimental investigation of a photovoltaic thermal collector with energy storage for power generation, building heating and natural ventilation, Renew. Energy 150 (2020) 12–22, https://doi.org/10.1016/j.renene.2019.12.112.
[8] C. Bott, I. Dressel, P. Bayer, State-of-the-technology review of water-based closed seasonal thermal energy storage systems, Renew. Sustain. Energy Rev. 113 (2019) 109241, https://doi.org/10.1016/j.rser.2019.06.048.
[9] I. Sarbu, C. Sebarchievici, A comprehensive review of thermal energy storage, Sustainability 10 (1) (2018) 191, https://doi.org/10.3390/su10010191.
[10] L. Ciappi, Y. Ding, A. Sciacovelli, Design of an innovative latent heat thermal energy storage prototype with pillow plates through analytical and computational fluid dynamics modelling, Comput. Therm. Sci. (2026), https://doi.org/10.1615/ComputThermalScien.2026063117.
[11] R. Baetens, B.P. Jelle, A. Gustavsen, Phase change materials for building applications: a state-of-the-art review, Energy Build. 42 (9) (2010) 1361–1368, https://doi.org/10.1016/j.enbuild.2010.03.026.
[12] M. Al-Maghalseh, K. Mahkamov, Methods of heat transfer intensification in PCM thermal storage systems: review paper, Renew. Sustain. Energy Rev. 92 (2018) 62–94, https://doi.org/10.1016/j.rser.2018.04.064.
[13] O. Bamisile, C. Acen, D. Cai, Q. Huang, I. Staffell, Environmental factors affecting solar photovoltaic output, Renew. Sustain. Energy Rev. 208 (2025) 115073, https://doi.org/10.1016/j.rser.2024.115073.
[14] M. Alharbi, R. Alahmadi, A. Alahmadi, Meteorological-data-based modeling for PV performance optimization, Sustainability 15 (11) (2023) 8659, https://doi.org/10.3390/su15118659.
[15] S. Alsaqoor, A. Alqatamin, A. Alahmer, Z. Nan, Y. Al-Husban, H. Jouhara, The impact of phase change material on photovoltaic thermal (PVT) systems: a numerical study, Int. J. Thermofluids 18 (2023) 100365, https://doi.org/10.1016/j.ijft.2023.100365.
[16] S. Preet, B. Bhushan, T. Mahajan, Experimental investigation of water based photovoltaic/thermal (PV/T) system with and without phase change material (PCM), Sol. Energy 155 (2017) 1104–1120, https://doi.org/10.1016/j.solener.2017.07.040.
[17] X. Yang, L. Sun, Y. Yuan, X. Zhao, X. Cao, Experimental investigation on performance comparison of PV/T-PCM system and PV/T system, Renew. Energy 119 (2018) 152–159, https://doi.org/10.1016/j.renene.2017.11.094.
[18] M.S. Hossain, A.K. Pandey, J. Selvaraj, N.A. Rahim, M.M. Islam, V.V. Tyagi, Two side serpentine flow based photovoltaic-thermal-phase change materials (PVT-PCM) system: energy, exergy and economic analysis, Renew. Energy 136 (2019) 1320–1336, https://doi.org/10.1016/j.renene.2018.10.097.
[19] T. Maatallah, R. Zachariah, F.G. Al-Amri, Exergo-economic analysis of a serpentine flow type water based photovoltaic thermal system with phase change material (PVT-PCM/water), Sol. Energy 193 (2019) 195–204, https://doi.org/10.1016/j.solener.2019.09.063.
[20] M.A. Vaziri Rad, A. Kasaeian, S. Mousavi, F. Rajaee, A. Kouravand, Empirical investigation of a photovoltaic-thermal system with phase change materials and aluminum shavings porous media, Renew. Energy 167 (2021) 662–675, https://doi.org/10.1016/j.renene.2020.11.135.
[21] V. Sun, A. Asanakham, T. Deethayat, T. Kiatsiriroat, Performance analysis on combined heat and power of photovoltaic-thermal module integrated with phase change material-water storage, J. Energy Storage 47 (2022) 103614, https://doi.org/10.1016/j.est.2021.103614.
[22] M.M. Islam, M. Hasanuzzaman, N.A. Rahim, A.K. Pandey, M. Rawa, L. Kumar, Real time experimental performance investigation of a NePCM based photovoltaic thermal system: an energetic and exergetic approach, Renew. Energy 172 (2021) 71–87, https://doi.org/10.1016/j.renene.2021.02.169.
[23] H. Fayaz, N.A. Rahim, M. Hasanuzzaman, R. Nasrin, A. Rivai, Numerical and experimental investigation of the effect of operating conditions on performance of PVT and PVT-PCM, Renew. Energy 143 (2019) 827–841, https://doi.org/10.1016/j.renene.2019.05.041.
[24] K. Huang, H. Lin, G. Feng, A. Li, H. Xie, J. Wei, Experimental and numerical thermal performance analysis of a phase change water tank with S-shaped channel, J. Energy Storage 108 (2025) 114840, https://doi.org/10.1016/j.est.2024.114840.
[25] B. Peng, W. Sheng, Z. He, H. Wang, F. Su, S. Wang, Systematic investigations on charging/discharging performances improvement of phase change materials by structured network fins, Energy 242 (2022) 122963, https://doi.org/10.1016/j.energy.2021.122963.
[26] G.S. Kumar, D. Nagarajan, L.A. Chidambaram, V. Kumaresan, Y. Ding, R. Velraj, Role of PCM addition on stratification behaviour in a thermal storage tank: an experimental study, Energy 115 (2016) 1168–1178, https://doi.org/10.1016/j.energy.2016.09.014.
[27] X. Yang, Q. Bai, Q. Zhang, W. Hu, L. Jin, J. Yan, Thermal and economic analysis of charging and discharging characteristics of composite phase change materials for cold storage, Appl. Energy 225 (2018) 585–599, https://doi.org/10.1016/j.apenergy.2018.05.063.
[28] A. Joseph, M. Kabbara, D. Groulx, P. Allred, M.A. White, Characterization and real-time testing of phase-change materials for solar thermal energy storage, Int. J. Energy Res. 40 (1) (2016) 61–70, https://doi.org/10.1002/er.3336.
[29] H.M. Teamah, M.F. Lightstone, J.S. Cotton, Potential of cascaded phase change materials in enhancing solar domestic hot water systems, Sol. Energy 159 (2018) 519–530, https://doi.org/10.1016/j.solener.2017.11.034.
[30] J. Zhao, Y. Ji, Y. Yuan, Z. Zhang, J. Lu, Energy-saving analysis of solar heating system with PCM storage tank, Energies 11 (1) (2018) 237, https://doi.org/10.3390/en11010237.
[31] R. Koželj, U. Mlakar, E. Zavrl, U. Stritih, R. Stropnik, Experimental and numerical analysis of an improved thermal storage tank with encapsulated PCM for retrofitted buildings, Energy Build. 248 (2021) 111196, https://doi.org/10.1016/j.enbuild.2021.111196.

[32] A. Castell, M. Belusko, F. Bruno, L.F. Cabeza, Maximisation of heat transfer in a coil-in-tank PCM cold storage system, Appl. Energy 88 (11) (2011) 4120–4127, https://doi.org/10.1016/j.apenergy.2011.03.046.
[33] M. Medrano, M.O. Yilmaz, M. Nogués, I. Martorell, J. Roca, L.F. Cabeza, Experimental evaluation of commercial heat exchangers for use as PCM thermal storage systems, Appl. Energy 86 (10) (2009) 2047–2055, https://doi.org/10.1016/j.apenergy.2009.01.014.
[34] A. Kazemian, M. Khatibi, S. Entezari, T. Ma, H. Yang, Efficient energy generation and thermal storage in a photovoltaic thermal system partially covered by solar cells and integrated with organic phase change materials, Renew. Sustain. Energy Rev. 188 (2023) 113705, https://doi.org/10.1016/j.rser.2023.113705.
[35] A. Hamada, M. Emam, H.A. Refaey, M. Moawed, M.A. Abdelrahman, Investigating the performance of a water-based PVT system using encapsulated PCM balls: an experimental study, Energy 284 (2023) 128574, https://doi.org/10.1016/j.energy.2023.128574.
[36] K.E. Park, W.J. Choi, H. Kim, J. Kim, J.Y. Hong, M.H. Kim, Investigation of the energy performance of thermal energy sharing for photovoltaic-thermal systems in a thermal prosumer network, Case Stud. Therm. Eng. 61 (2024) 104881, https://doi.org/10.1016/j.csite.2024.104881.
[37] B. Peng, G. Huang, P. Wang, W. Li, W. Chang, J. Ma, C. Li, Effects of thermal conductivity and density on phase change materials-based thermal energy storage systems, Energy 172 (2019) 580–591, https://doi.org/10.1016/j.energy.2019.01.147.
[38] R.K. Rajamony, A.K. Pandey, A.G.N. Sofiah, M.A. Wadaan, J.K.S. Paw, S.S. Kousik, A. Baabbad, M. Samykano, V. Paranthaman, Energizing the thermophysical properties of phase change material using carbon-based nano additives for sustainable thermal energy storage application in photovoltaic thermal systems, Mater. Today Sustain. 25 (2024) 100658, https://doi.org/10.1016/j.mtsust.2023.100658.
[39] K.K. Gupta, P.K.S. Rathore, B.S. Sikarwar, A.K. Pandey, Solar to thermal energy storage performance of composite phase change material supported by copper foam loaded with graphite and boron nitride, Sol. Energy 272 (2024) 112459, https://doi.org/10.1016/j.solener.2024.112459.
[40] Y. An, J. Kim, H.J. Joo, W.J. Lee, G. Han, H. Kim, M.-H. Kim, Experimental performance analysis of photovoltaic systems applied to a positive energy community based on building renovation, Renew. Energy 219 (2023) 119369, https://doi.org/10.1016/j.renene.2023.119369.
[41] W.J. Choi, W. Lee, D.-W. Kim, Y. An, H.J. Joo, J.Y. Hong, M.-H. Kim, Experimental investigation of the energy performance of a photovoltaic-thermal assisted ground source heat pump system for net plus energy houses, Case Stud. Therm. Eng. 69 (2025) 105974, https://doi.org/10.1016/j.csite.2025.105974.
[42] Y. An, J. Kim, H.J. Joo, W. Lee, G. Han, H. Kim, M.-H. Kim, Retrofit of renewable energy systems in existing community for positive energy community, Energy Rep. 9 (2023) 3733–3744, https://doi.org/10.1016/j.egyr.2023.02.055.
[43] G. Han, Y.S. An, J.K. Kim, D.E. Jung, H.J. Joo, H. Kim, M.-H. Kim, Analysis of grid flexibility in 100% electrified urban energy community: a year-long empirical study, Sustain. Cities Soc. 113 (2024) 105244, https://doi.org/10.1016/j.scs.2024.105648.
[44] S.J. Kline, F.A. McClintock, Describing uncertainties in single-sample experiments, Mech. Eng. 75 (1) (1963) 3–8.